REPORT DOCUMENTATION PAGE

Form Approved OMB NO. 0704-0188

1. REPORT DATE (DD-MM-YYYY)	2. REPORT TYPE	3. DATES COVERED (From - To)
	New Reprint	-

4. TITLE AND SUBTITLE	5a. CONTRACT NUMBER
Influence of microstructure on micro-/nano-mechanical measurements of select model transparent poly(urethane urea) elastomers	
	5b. GRANT NUMBER
	W911NF-13-D-0001
	5c. PROGRAM ELEMENT NUMBER
	611104

6. AUTHORS	5d. PROJECT NUMBER
Kenneth E. Strawhecker, Alex J. Hsieh, Tanya L. Chantawansri, Z. Ilke Kalcioglu, Krystyn J. Van Vliet	
	5e. TASK NUMBER
	5f. WORK UNIT NUMBER

7. PERFORMING ORGANIZATION NAMES AND ADDRESSES	8. PERFORMING ORGANIZATION REPORT NUMBER
Massachusetts Institute of Technology (MIT) Office of Sponsored Programs 77 Massachusetts Avenue Cambridge, MA 02139 -4307	

9. SPONSORING/MONITORING AGENCY NAME(S) AND ADDRESS(ES)	10. SPONSOR/MONITOR'S ACRONYM(S)
U.S. Army Research Office P.O. Box 12211 Research Triangle Park, NC 27709-2211	ARO
	11. SPONSOR/MONITOR'S REPORT NUMBER(S)
	63760-CH-ISN.45

12. DISTRIBUTION AVAILIBILITY STATEMENT

Approved for public release; distribution is unlimited.

13. SUPPLEMENTARY NOTES

14. ABSTRACT

Morphology of 4,40 -dicyclohexylmethane diisocyanateepoly(tetramethylene oxide) (PTMO)ediethyl toluenediamine based poly(urethane urea) (PUU) elastomers is investigated by atomic force micros- copy (AFM) and compared with elastic modulus data measured from AFM-enabled indentation, dynamic nanoindentation (nanoDMA), and dynamic mechanical analysis (DMA). These measurements highlight the effect of altering the molecular weight (Mw) of PTMO, which is used as a soft segment (SS), on the microstructure. In particular, at SS

15. SUBJECT TERMS

Poly(urethane urea), AFM, Morphology, elastomers

16. SECURITY CLASSIFICATION OF:			17. LIMITATION OF ABSTRACT	15. NUMBER OF PAGES	19a. NAME OF RESPONSIBLE PERSON
a. REPORT	b. ABSTRACT	c. THIS PAGE			John Joannopoulos
UU	UU	UU	UU		19b. TELEPHONE NUMBER
					617-253-4806

Report Title

Influence of microstructure on micro-/nano-mechanical measurements of select model transparent poly(urethane urea) elastomers

ABSTRACT

Morphology of 4,40 -dicyclohexylmethane diisocyanateepoly(tetramethylene oxide) (PTMO)ediethyl toluenediamine based poly(urethane urea) (PUU) elastomers is investigated by atomic force micros- copy (AFM) and compared with elastic modulus data measured from AFM-enabled indentation, dynamic nanoindentation (nanoDMA), and dynamic mechanical analysis (DMA). These measurements highlight the effect of altering the molecular weight (Mw) of PTMO, which is used as a soft segment (SS), on the microstructure. In particular, at SS Mw 2000 g/mol, a strong microphase-separated morphology is observed, whereas a phase-mixed dominated microstructure is noted in PUU with SS Mw of 1000 and 650 g/mol. These observations are also consistent with DMA tan d results. Furthermore, instrumented impact indentation is also utilized for elucidation of dynamic damping characteristics in these PUUs.

REPORT DOCUMENTATION PAGE (SF298)
(Continuation Sheet)
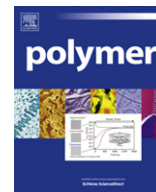
Continuation for Block 13

ARO Report Number   63760.45-CH-ISN
Influence of microstructure on micro-/nano-mech   ...

Block 13: Supplementary Note

Influence of microstructure on micro-/nano-mechanical measurements of select model transparent poly(urethane urea) elastomers

Kenneth E. Strawhecker [a,*], Alex J. Hsieh [a], Tanya L. Chantawansri [a], Z. Ilke Kalcioglu [b], Krystyn J. Van Vliet [b]

[a] U.S. Army Research Laboratory, RDRL-WMM-G, Aberdeen Proving Ground, MD 21005-5069, USA
[b] Department of Materials Science and Engineering, Massachusetts Institute of Technology, Cambridge, MA 02139, USA

ABSTRACT

Morphology of 4,4′-dicyclohexylmethane diisocyanate–poly(tetramethylene oxide) (PTMO)–diethyl toluenediamine based poly(urethane urea) (PUU) elastomers is investigated by atomic force microscopy (AFM) and compared with elastic modulus data measured from AFM-enabled indentation, dynamic nanoindentation (nanoDMA), and dynamic mechanical analysis (DMA). These measurements highlight the effect of altering the molecular weight (M_w) of PTMO, which is used as a soft segment (SS), on the microstructure. In particular, at SS M_w 2000 g/mol, a strong microphase-separated morphology is observed, whereas a phase-mixed dominated microstructure is noted in PUU with SS M_w of 1000 and 650 g/mol. These observations are also consistent with DMA tan δ results. Furthermore, instrumented impact indentation is also utilized for elucidation of dynamic damping characteristics in these PUUs.

Published by Elsevier Ltd.

1. Introduction

Elastomers are versatile materials that are vital to a broad range of industrial, medical, and military applications, particularly in the areas of coating, adhesives, foams, and composite structures [1]. More specifically, high performance polyurea and poly(urethane urea) (PUU) elastomers have recently gained considerable interest throughout the Department of Defense (DoD) particularly for their potential in ballistic impact protection and blast mitigation capabilities [2–5]. Under high-rate loading conditions, the physical response of this class of material can be tailored to transition from the rubbery-like to the leathery-like or the glassy regime with increasing strain-rate, where stress levels may be greatly enhanced and large energy-dissipation mechanisms can be realized [2,6–10].

The self-assembly of hard segments in polyurethanes, PUUs and polyureas is known to be very complex. However, it is well-recognized that the strong intermolecular hydrogen bonding between the urethane groups as well as between the urea groups plays an important role, though not necessarily a prerequisite [11], on the microphase separation among these elastomers. Even so,

hydrogen bonding is prevalent in the domains that form from the segregation of hard segments, which act as physical cross-links for the elastomer. In addition to the effect of hydrogen bonding, the influence of microstructure on thermal and mechanical properties of these microphase-separated elastomers has also been extensively investigated [12–32]. Earlier studies have shown that changing miscibility between hard and soft segments through the choice of either polar or highly apolar macrodiols as the soft segment causes a drastic difference in the degree of microphase separation [14–16]. Yilgor et al. also revealed structure–morphology–property relations in a comprehensive evaluation of non-chain extended polyurethanes and polyureas, where polyureas exhibited greater tendency towards microphase separation than the corresponding polyurethane analogs, and stronger hydrogen bonding between the urea groups was regarded as an important attribute [16].

Recent studies of select model 4,4′-dicyclohexylmethane diisocyanate (HMDI)–poly(tetramethylene oxide) (PTMO)–diethyltoluenediamine (DETA) based PUU elastomers have clearly demonstrated the composition dependence of tunable microstructure [29–31]. Altering the molecular weight (M_w) of PTMO, the choice of soft segment (SS), from 2000 (2K) to 1000 (1K) g/mol while keeping the molar ratio of HMDI:PTMO:DETA constant (2:1:1) gave rise to a change in scattering characteristics observed via small-angle X-ray scattering (SAXS). An increase in SS glass transition temperature

* Corresponding author. Tel.: +1 410 306 2147; fax: +1 410 306 0676.
E-mail address: kenneth.e.strawhecker.civ@mail.mil (K.E. Strawhecker).

(T_g) and a broadening of the SS relaxation were also noted based on the loss-tangent relaxation data obtained from dynamic mechanical analysis (DMA) [29–31]. PUUs consisting of PTMO with M_w of 1000 g/mol (PUU 1K) also exhibited greater strain-rate sensitivity and a drastic improvement in permeation resistance against chloroethyl ethyl sulfide, a simulant for the chemical warfare blister agent than the corresponding PUU analogs with PTMO M_w of 2000 g/mol (PUU 2K) [29–31]. This included significantly longer breakthrough time and slower steady-state flux than corresponding PUU 2K materials of similar hard segment (HS) contents [30,31].

There have also been several studies on the *in-situ* microstructure characterization of polyurethane, PUU and polyurea elastomers upon mechanical deformation using synchrotron radiation along with SAXS, wide-angle X-ray diffraction and time-resolved Fourier transform infrared spectroscopy [28,33,34]. However, the challenges for the rational design of hierarchical elastomeric materials to achieve a simultaneous improvement in dynamic mechanical strength and chemical barrier properties, which are critical for the next-generation protective system applications, reside on the realization of the key physical events that occur on various temporal and spatial scales. Quantitative characterization of phase structure across the length scales could provide better insight for correlation of microstructure and properties.

In this work, atomic force microscopy (AFM) analysis is utilized to first ascertain the microstructure of select model PUUs. AFM is a well-recognized method that has been used for the characterization of microstructure in various polymers, including segmented elastomers such as polyurethanes, PUUs and polyureas [15–27,32]. In contrast to SAXS, AFM is capable of providing real-space visual characterization of the organization, dimension, shape, and dispersion of the lamellar hard segments and hard segment domains in microphase-separated elastomers [14–17,19–21,27]. AFM-modulus mapping, unlike the common AFM-phase imaging approach, is a relatively new technique. Whereas AFM-phase images are only qualitative in nature, images that display the elastic modulus at each image point (AFM-modulus images) are quantitative. Even so, results from AFM-phase and AFM-modulus images have been shown to be consistent [35], where consistency has also been observed between different AFM-modulus mapping techniques such as HarmoniX™ imaging and Peak Force Tapping™ [36]. In this manuscript, the molecular influence on elastic modulus measured via AFM will be compared with those obtained from both dynamic nanoindentation and dynamic mechanical analysis. Additionally, instrumented impact indentation, capable of differentiating the dynamic impact response, is included to elucidate the influence of microstructure on damping characteristics among these PUU elastomers.

2. Experimental

2.1. Materials

Select model PUU materials composed of 4,4′-dicyclohexyl-methane diisocyanate (HMDI–Desmodur W, Bayer MaterialScience), diethyltoluenediamine (DETA–Ethacure® 100-LC, Albemarle Corporation, Baton Rouge, Louisiana), and poly(tetramethylene oxide) (PTMO–PolyTHF, BASF Corporation) were chosen for this study. Three different M_ws of PTMO, 650, 1000 and 2000 g/mol, were used in the PUU synthesis. The PUU elastomers were prepared via a two-step, pre-polymer synthesis method [29]. First, PTMO, the soft segment, was reacted with HMDI to form a pre-polymer with a urethane linkage, and the reaction was carried out to ensure PTMO was completely end-capped with diisocyanate groups. HMDI was weighed and heated to 65 °C in a dried round-bottom flask in a nitrogen environment. In a separate container,

PTMO was accurately weighed and mixed thoroughly with a tin catalyst and the mixture was then held at 45–50 °C. The PTMO/tin mixture was then added to the HMDI and blended using a standard laboratory scale mechanical overhead stirrer, during which the temperature reached about 120 °C as a result of the exothermic reaction. After the exotherm subsided, the mixture was heated in an external oil bath and held at 130–135 °C for several hours. The reaction mixture was then cooled and allowed to stand overnight at room temperature. Next, prior to the PUU synthesis, the pre-polymer was heated to 150 °C for a minimum of 30 min, and then cooled down to 65 °C while being slowly stirred and degassed in a vacuum chamber. This pre-polymer was then reacted with the DETA to complete polymerization. The reaction of HMDI with the DETA diamine resulted in hard segments with urea linkages. Since the reaction rate was extremely rapid, the pre-weighed DETA was introduced into the pre-polymer using a syringe. This was followed by a thorough and rapid mixing, and then by degassing for ∼1 min. An *in-situ* polymerization/as-cast approach was utilized, wherein the resulting mixture of pre-polymer and DETA was poured into molds formed between two glass plates and allowed for completion of cure overnight at 110 °C. As a result, thin films or sheets of requisite thicknesses were fabricated directly from this *in-situ* synthesis/processing method.

In this study, PUUs of the molar ratio 2:1:1 of diisocyanate:diamine chain extender:PTMO are used in the AFM microstructure analyses. In the sample nomenclature, the numerals '*xyz*' refer to the molar ratio of diisocyanate:diamine chain extender:PTMO, and the succeeding '650,' '1K' and '2K' refer to the M_w of PTMO as 650, 1000 and 2000 g/mol, respectively. PUU consisting of PTMO with M_w of 1000 g/mol and with the molar ratio 3:2:1 is also included in the impact indentation measurement. The HS content used in this work only accounts for the portion of diisocyanate that reacts with diamine and is calculated by following equation (1) [23]:

$$\% \, HS_u = \frac{100(R-1)(M_{di} + M_{da})}{(M_g + R(M_{di}) + (R-1)(M_{da}))} \tag{1}$$

where R is the molar ratio of the diisocyanate to PTMO, and M_{di}, M_{da} and M_g are the number average molecular weights of HMDI, DETA and PTMO, respectively. Table 1 lists the composition including the molar ratio, the SS molecular weight, and wt.% of hard segment of PUUs studied in this work.

2.2. Instrumentation

2.2.1. Atomic force microscopy

Both AFM-phase imaging and AFM-modulus imaging were utilized in this study. The HarmoniX™ technique was used to simultaneously acquire AFM-modulus and AFM-phase images. Imaging was performed using a Dimension 3100 AFM with a Nanoscope V controller in either standard tapping mode or modulus mapping mode. Commercial AFM tips (RTESP and HMX from Bruker-Nano, formerly Veeco) were used as received. Tapping-mode images were obtained using the standard mode-1 resonant frequency of the RTESP probes, nominally 311–355 kHz

Table 1
Composition and hard segment content of select PUU materials.

	Molar ratio of [HMDI]:[DETA]:[PTMO]	M_w (g/mol) of PTMO	Wt.% of hard segment content HS_u
211-650	2:1:1	650	33
211-1K	2:1:1	1000	26
211-2K	2:1:1	2000	16
321-2K	3:2:1	2000	28

and spring constant in the range of 20–80 N/m. For these studies, an amplitude set-point of 70–80% of the free-air oscillation amplitude was employed with a scan rate of 0.25–1.0 Hz. Elastic modulus was determined using the Veeco HarmoniX™ software. The HMX probes were calibrated prior to each scan using a standard sample composed of a copolymer of polystyrene and low-density polyethylene (PS–LDPE), following the calibration method outlined previously [37]. Elastic modulus values obtained from this scanning method were determined using image or region averaging (roughness analysis command) as well as section analysis (both in the standard Veeco analysis software, V7.30r1Sr3). AFM-modulus values were obtained by averaging absolute pixel values across the AFM-modulus image. (Some AFM-phase images shown in this work may be presented after applying standard image flattening techniques.)

Since AFM-modulus mapping is a relatively new technique, the error analysis and reproducibility of measurement were also included in this study. In the course of these AFM-modulus experiments, it was found that the absolute error or deviation of AFM-modulus values for a given sample was in the range of 200–300 MPa, which was ∼100% of the mean elastic modulus for compliant samples (200 MPa) and ∼20% of the mean elastic modulus for stiff samples (1.5 GPa). The experiments were repeated with changes in scan region, scan size, and HMX probe. There was no trend when moving to a new scan region, as should be expected, provided obvious surface defects were avoided. No trend was observed when varying scan size, except that at larger scan sizes (lower resolution) *distinct* microstructural features were not detected. Qualitatively, there was more variability in the AFM-modulus measurement from probe-to-probe, compared with other changes such as scan size or moving to a new spot on the same sample. Initially, it was assumed that the tip shape would not change over several scans in different regions or on different samples. However, it became apparent that the change in tip shape was an issue. This was addressed by scanning the reference sample in between each sample scan so that the tip shape could be recalculated using the standard technique.

2.2.2. Instrumented nanoindentation

Nanoscale dynamic mechanical analysis (nanoDMA) was performed using a TI-950 TriboIndenter (Hysitron) equipped with a Berkovich diamond probe with a nominal tip radius of curvature of approximately 100 nm. In this experiment, a quasi-static load of 1500 μN was superposed with a dynamic load of 3 μN, where the dynamic load was chosen such that it resulted in a dynamic displacement amplitude of typically 0.5–1.0 nm. Following a drift measurement (which was done at a preload of 1.0 μN for 20 s prior to each indent, where a correction was applied to the displacement data), the quasi-static loading rate was 100 μN/s. Once the maximum quasi-static load was reached, the frequency was then varied from 10 to 300 Hz over 30 equally sized steps.

2.2.3. Dynamic mechanical analysis

The DMA measurements were performed on a TA Instruments Q800 Dynamic Mechanical Analyzer. The PUU samples with dimension of 2 mm width, 1 mm thickness and about 10 mm gauge length were tested in an oscillatory tensile mode from −100 °C to 150 °C at a heating rate of 1 °C/min and at a frequency of 1 Hz.

2.2.4. Instrumented impact indentation

Pendulum-based impact experiments were conducted via a commercially available instrumented indenter (Micro Materials, Ltd.) utilizing a Berkovich probe. Details of the instrumentation and experimental procedure were described previously in Refs. [38–40]. The probe displacement vs. time response was recorded

throughout successive impact cycles until the probe came to a full rest on sample surface, and impact indentation velocity vs. time response was calculated as the time derivative of displacement. Impact velocities (v_{in}), and maximum penetration depths (x_{max}) which correlated with impact indentation resistance (i.e. higher x_{max} corresponds to lower impact indentation resistance) were calculated utilizing both displacement and velocity responses as described previously [40]. Impact indentation experiments were conducted at impact velocities ranging 1–5.5 mm/s corresponding to strain rates of ∼50–200 s^{-1} approximated as ∼v_{in}/x_{max}. Per impact velocity, three replicate experiments were carried out for each PUU composition and data were reported as mean ± standard deviation.

3. Results and discussion

3.1. Microstructure

AFM imaging was conducted on both the free surface of as-cast PUUs and the bulk of microtomed samples to investigate the microstructure as a function of SS molecular weight. In this work, the term "bulk" is used to describe microtomed surfaces as opposed to "surface" which refers to the top surface of a prepared film, unless otherwise noted. The sample preparation of these bulk samples is as follows: select PUUs were prepared by microtoming using a Leica ultracut UCT with EM FCS cryochamber at −80 °C for the 211-2K and −50 °C for the 211-1K and 211-650 samples.

Fig. 1 is a set of low (a–c) and high (d–f) magnification AFM-modulus images showing the bulk microstructure details of the (a,d) 211-2K, (b,e) 211-1K and (c,f) 211-650. AFM-phase images capture the same microstructural details and were omitted for brevity. For these AFM-modulus images the scale is 2.5 GPa (light-to-dark). Bright AFM-modulus data corresponds to stiffer sample regions, suggesting 211-650 has the greatest stiffness among all (Fig. 1c and f). From these AFM images, the effect of altering the SS molecular weight on microstructure can be visualized. First, considering Fig. 1a–c, which are the low magnification images, there are longitudinal scratch features present in the 211-1K and the 211-650 which are artifacts of microtoming. These are not present in the 211-2K sample because the 211-2K sample is much more compliant and able to recover from the microtome preparation unlike the 211-650 and 211-1K samples. When the scan region was chosen for the higher magnification images of Fig. 1, it was done such that the scan region was in between these microtome knife scratches resulting in images (Fig. 1c,d,f) which show primarily bulk microstructure with little presence of microtoming artifacts. The 211-2K sample is mostly microphase-separated with the presence of some irregularly-shaped rod-like features. As the SS M_w decreases from 2000 g/mol to the 1000 g/mol and 650 g/mol, the extent of phase mixing between the hard and soft segments increases. No evidence of crystallinity was noted in these PUU elastomers from either DSC or wide-angle X-ray scattering (WAXS) (not shown), where results from the latter indicated only a broad halo with a Bragg spacing of ∼4.4 Å, confirming the amorphous characteristics of our PUU systems [29]. It is also noteworthy that 211-2K appears to be slightly translucent while both 211-1K and 211-650 are completely transparent, which can be attributed to the extent of phase mixing.

To fully understand the microstructure of these materials AFM-modulus and AFM-phase scans of the as-cast surface were also performed. Distinct microstructural features, not found in the microtomed, bulk regions, were observed on the surface of these materials. Fig. 2 highlights the morphological features of the surfaces of each of the samples using AFM-phase images which are often consistent with AFM-modulus images (see also Fig. 4). The
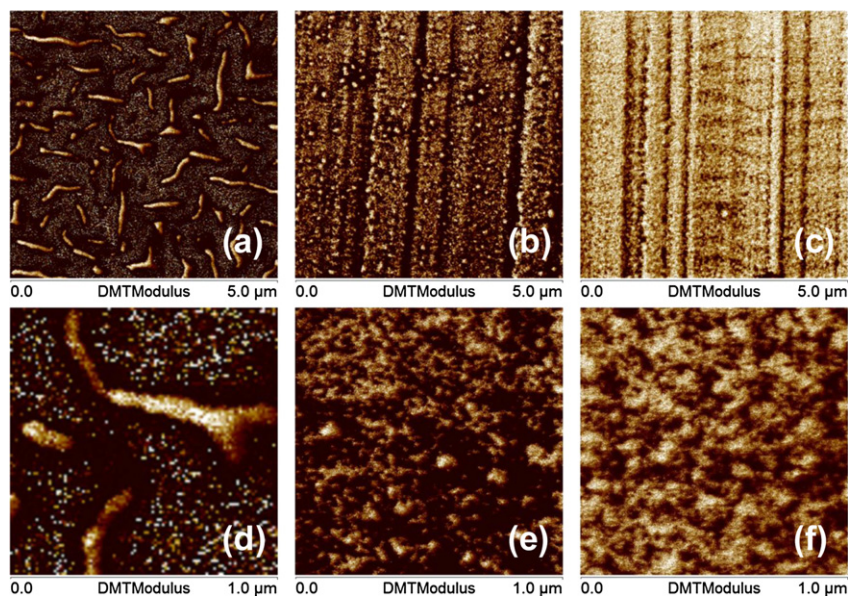
Fig. 1. AFM-modulus images (2.5 GPa light-to-dark) showing distinctly different microstructure features for (a,d) 211-2K, (b,e) 211-1K, and (c,f) 211-650. Longitudinal lines in (b) and (c) are from the microtoming preparation. Images are 5 × 5 μm (a–c) and 1 × 1 μm (d–f).

top row of Fig. 2 shows 5 × 5 μm AFM-phase images of the 211-2K [41] (left), the 211-1K [41] (middle) and the 211-650 (right), whereas the bottom row shows regions of these at higher magnifications (1 × 1 μm, and left-middle-right, respectively). Admittedly these regions may include process-induced surface morphologies not native to the bulk, though these features are consistently found on the surface and are reminiscent of PUU morphologies found elsewhere [16,26]. Specifically, in the case of the 211-1K sample (Fig. 2e) features include 1) hard domain regions consisting of rod-like lamellar hard segments oriented in parallel, which grow in long stacks or may lie next to each other to form irregularly-shaped hard

domains; 2) a matrix consisting of predominantly phase-mixed hard and soft segments, stiff (bright) in AFM-phase, wherein the hard segments form fibrillar-like structures (see arrows). This fibrillar-like feature may consist of hard segments interacting to form non-lamellar stiff regions oriented parallel to the polymer chains as depicted schematically in Fig. 3 (left) [34,42]. The rod-like lamellar hard segments are presumably formed through the self-assembly of hard segments with the domain axis (or the long period) oriented perpendicular to the polymer chains [34,42], as can be seen in Fig. 3 (right). Measurements of typical needle-like
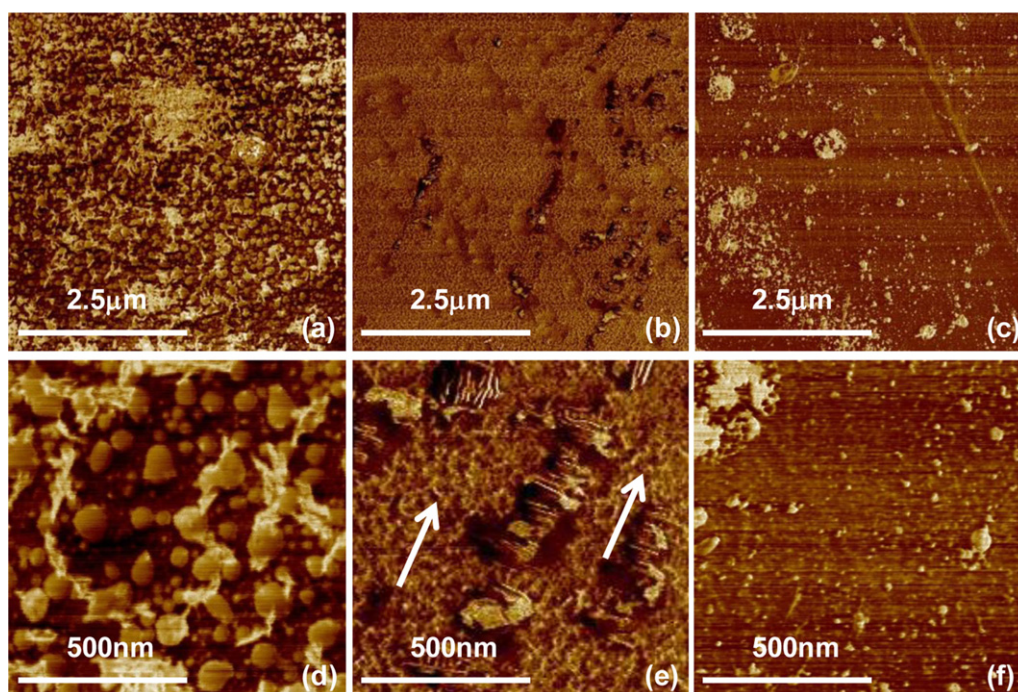

Fig. 2. AFM-phase images at low (a–c: 5 × 5 μm) and high (d–f: 1 × 1 μm) magnification of (a,d) 211-2K (75° light-to-dark), (b,e) 211-1K (30° light-to-dark) and (c,f) 211-650 (30° light-to-dark). The needle-like features in the 211-1K image (e) are about 10 nm in width with about 5–10 nm separation.
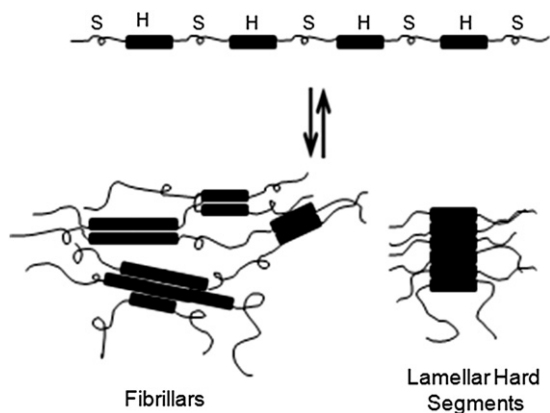
Fig. 3. A schematic of hard segments in the form of fibrillars in the amorphous, phase-mixed matrix vs. well-organized lamellar hard segments, (H and S denote hard and soft segments, respectively) in accordance with previous work [34].

individual hard segments are about 10 nm in width, with a spacing of about 5–10 nm.

It is noteworthy that despite differences in the surface and bulk microstructure, the microphase separation exhibited by 211-2K is distinctive from that observed in 211-1K. For instance, the microstructure for the bulk of 211-2K is composed of isolated rod-like hard segment domains (Fig. 1a and d) or particulate-like microstructure features on the surface (Fig. 2d), whereas a predominantly fibrillar-like microstructure is seen in 211-1K (Fig. 2e), with greater phase-mixed features on the bulk (Fig. 1e). Note that the size of these irregularly-shaped rod-like microstructures seen in the bulk in 211-2K (~75–140 nm, Fig. 1a and d), though comparable to the dimensions of the particulate-like features seen in Fig. 2a and d, is significantly larger than any of the features observed in 211-1K (Figs. 1 and 2b and e).

These observations indicate that there can be some discrepancy between the surface morphology and the bulk microstructure. This is presumably due to a variation in reaction kinetics across the thickness as well as a result of quenching which presumably favors demixing toward surface layers. For the latter, close contact of the as-cast surface with the glass plates, which were used in the *in-situ* polymerization/as-cast process, can induce quenching upon polymerization and contribute to the variations in the surface morphology.

Because of the higher degree of microphase separation in the 211-2K sample, the bulk AFM-phase and AFM-modulus images are investigated in more detail in Fig. 4. Fig. 4a has an AFM-phase scale of 50° (light-to-dark) and clearly shows the large stiff (bright) rod-like features already mentioned in Fig. 1a and d. Interestingly, the compliant (dark) matrix appears to be comprised of regions which are slightly more compliant (darker) and regions that are slightly less compliant (slightly less dark.) When focusing on the detail of the AFM-modulus image (Fig. 4b, note the log scale) it is apparent that the sample morphology indeed consists of not only very stiff rod-like features already mentioned, but also a compliant matrix which contains regions of varying stiffness composed of both SS-rich and phase-mixed regions. The presence of the phase-mixed regions, not prevalent in the SAXS data [29–31], corroborates well with the DMA results (see below).

3.2. Extent of phase mixing

An important element of the morphology, which has been linked to improved mechanical and barrier properties [29–31,42], is the presence of a phase-mixed hard and soft segment matrix. Based on AFM images this phase-mixed matrix is more prevalent in 211-1K and 211-650, but not as predominant in 211-2K which instead has a matrix composed of both SS-rich and phase-mixed regions. This phase mixing is due to an increase in the propensity for intermolecular hydrogen bonding with increasing hard segment content or decreasing PTMO M_w [29–31]. AFM images are able to discern the effect of molecular influence on the microstructure among these model PUU elastomers, where the extent of phase mixing is expected to affect the SS relaxation and the overall mechanical properties of PUUs.

In this work, DMA tan δ was also used to qualify the extent of phase mixing. Fig. 5 is a plot of loss-tangent (tan δ) data comparing the shift of SS T_g as well as the breadth of the relaxation with respect to varying the M_w of PTMO. For 211-2K there is a very distinct and intense relaxation at about −63 °C along with a weak shoulder. The relaxation peak presumably corresponds to the SS-rich amorphous matrix, while the weak shoulder may be associated with the sparsely populated phase-mixed regions. Broadening of the SS relaxation is evidenced as the M_w of PTMO decreases, indicative of phase mixing. This agrees with AFM, which notes the presence of an amorphous matrix consisting of predominantly fibrillar-like and phase-mixed microstructures in 211-1K and 211-650.
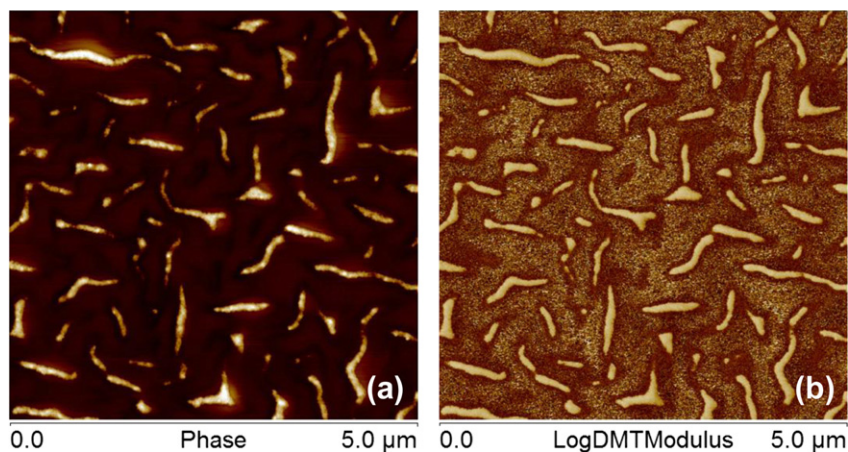

Fig. 4. 5 × 5 μm. a) AFM-phase (50° light-to-dark) and b) AFM-modulus (10 kPa–1 GPa light-to-dark, log scale) images of the 211-2K microphase-separated sample showing the consistency between the AFM-phase and AFM-modulus techniques while also highlighting the ability of AFM-modulus mapping to show very detailed distinct microstructures which are not as prevalent in the AFM-phase image.
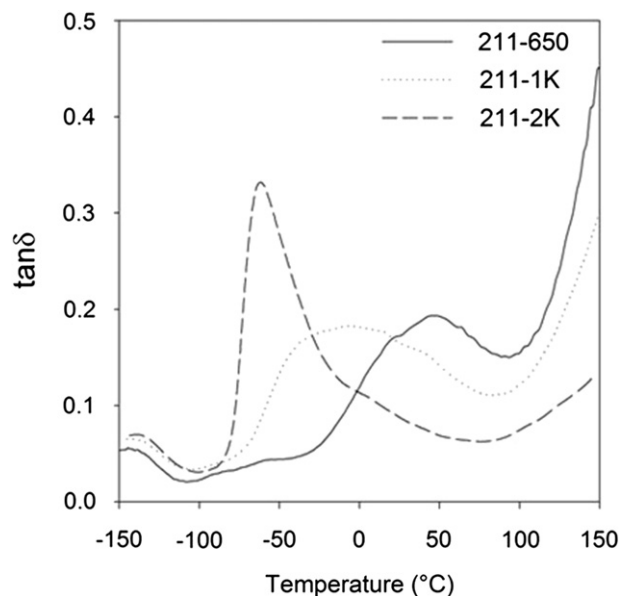
Fig. 5. DMA tan δ data for 211-650, 211-1K, and 211-2K PUUs.

3.3. Effect of microstructure on properties

The clear and distinctive microstructural features observed through AFM could affect the material properties of the select model PUUs. Fig. 6 is a plot of the average AFM-modulus values obtained from averaging the modulus values across all of the features within 10 μm scan regions on the surface and 15 μm scan regions in the bulk of each 211-series PUU sample. The large scan sizes were chosen in an attempt to get good averaging over the scan regions. The RMS deviation of the AFM-modulus value for pixels across any given image ranged from 400 to 600 MPa, regardless of the sample. The standard deviation between images at different spots on a single sample was about 30% for the stiffer samples (211-650 and 211-1K) and 65% for the 211-2K (more compliant sample), consistent with other studies [35].

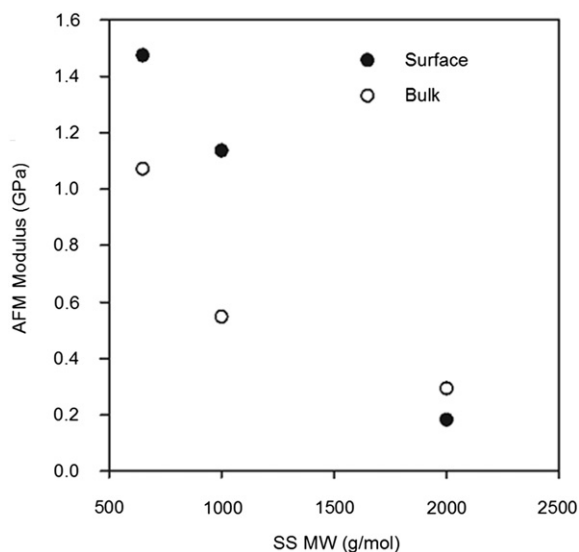As SS length increases, the AFM-modulus decreases for both the bulk and surface images. This indicates that 211-2K is more compliant than both 211-1K and 211-650. These trends are consistent with the composition dependence of the storage modulus obtained from DMA, which shows that the storage modulus at ambient temperature decreases in the order: 211-650 > 211-1K > 211-2K [30,31]. This is a result of both composition and physical (SS T_g) effects. The apparent difference in storage modulus is greater than an order of magnitude between 211-650 and 211-2K, 325 MPa vs. 22 MPa [30,31], respectively. Correspondingly, the AFM-modulus of the bulk is 1.07 GPa for 211-650 vs. 290 MPa for 211-2K.

The AFM-modulus values are consistently greater than those from DMA. To validate these differences, instrumented nano-indentation (nanoDMA) was also performed on select PUUs. Fig. 7 shows the storage modulus from nanoDMA for the 211-2K, 211-1K, and 211-650 as a function of frequency. First, it is apparent that the overall storage modulus at any given frequency decreases in the order: 211-650 > 211-1K > 211-2K. This is partly a function of higher hard segment content and the higher (and closer to room temperature) SS T_g for 211-650 as compared to the other model PUUs. As a result, 211-650 exhibits a greater increase of storage modulus with respect to frequency. The variation in apparent storage modulus can also be related to the microstructure where the 211-2K sample exhibits an SS-rich amorphous region as its matrix as opposed to the 211-1K and 211-650 samples, which have increasing amounts of the phase-mixed amorphous phase (Figs. 1 and 2).

The AFM-modulus data also agree with storage modulus data obtained through nanoDMA, a technique somewhat more representative of overall bulk material properties because of its probe depth and contact radius (approximately 1–10 and 3–30 microns, respectively). These results are also consistent with the trend in the storage modulus obtained from dynamic mechanical analysis (DMA) at a frequency of 1 Hz. The elastic modulus inferred from AFM-modulus images tends to be slightly higher than both the nanoDMA storage modulus and DMA storage modulus, which is partly a result of the differences in probe size or contact area (nanoDMA ∼ 100 μm²; AFM-modulus ∼ 50–100 nm²) but is greatly accentuated due to the rate-dependent characteristic of PUUs (1 Hz in DMA and ∼100 Hz in nanoDMA vs. ∼10⁵ Hz in AFM).

To further examine the rate-sensitivity of these elastomers at the nano-/micro-scale, we also exploit a unique pendulum-based

Fig. 6. The average AFM-modulus as a function of soft segment molecular weight for bulk (○) and surface (●) scan regions.
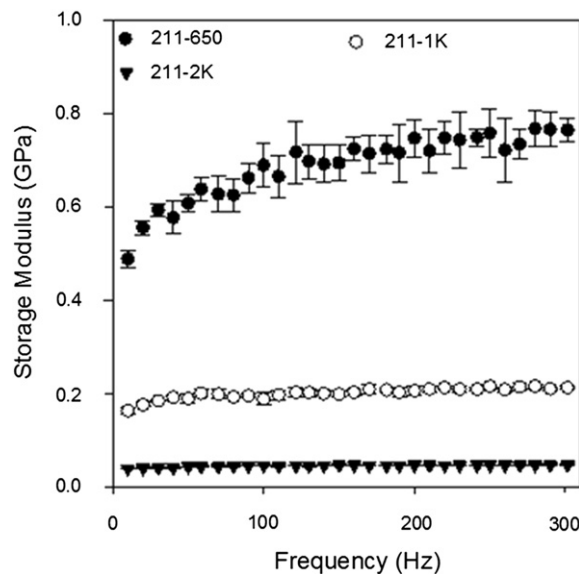

Fig. 7. NanoDMA (instrumented indentation) storage modulus as a function of frequency for 211–650 (●), 211-1K (○), and 211-2K (▼).

impact indentation. Measurements were performed by utilizing a Berkovich probe for determination of the maximum penetration depths, which is considered as a metric for impact resistance as well as impact indentation damping experienced in each of these PUU elastomers as a function of impact velocity. In Fig. 8, 211-650 as expected exhibits the highest impact resistance (i.e. lowest penetration depth) while 211-2K shows the least resistance to impact (largest penetration depth) among all PUU samples considered. This difference in the impact resistance is enhanced at higher impact velocities. When comparing PUUs of similar hard segment content, the results show that 211-1K and 321-2K (HS$_u$% of 26 wt.% and 28 wt.%, respectively) exhibit very similar maximum penetration depths at all the impact velocities explored herein.

In addition to comparing impact resistance, we also investigate the raw displacement time responses of the pendulum qualitatively with an attempt to further discern the dynamic damping characteristics among these PUU elastomers. Fig. 9 highlights the representative displacement vs. time responses at an impact velocity ~5.5 mm/s. For the 211-series PUUs, decreasing M_w of PTMO gives rise to enhanced damping in terms of the time duration required for full energy-dissipation; sample 211-650 exhibits the fastest damping by this measure. This relatively faster damping of an impact load can be attributed to two factors: (1) the SS T_g of 211-650 from DMA is much closer to ambient temperature; and (2) the presence of an amorphous, highly interconnected hydrogen-bonded network in 211-650, which could also facilitate the speed and extent of damping.

Increasing the HS content while keeping the PTMO M_w constant also has an effect on damping; 321-2K appears to dissipate energy slightly faster than 211-2K (Fig. 9), in addition to better resistance to impact indentation (Fig. 8). Fig. 10 is an AFM-phase image of 321-2K which displays much different surface morphology than the microstructure seen in 211-2K (Fig. 1d); the extent of phase mixing is apparently greater as a result of higher HS content in the former. This is consistent with the DMA tan δ data reported in [29–31]. Furthermore, 211-1K reveals greater damping response (i.e. dissipates the total energy faster) than 321-2K despite their similar HS contents and comparable maximum impact indentation depths. This is attributed to a higher T_g and greater phase mixing in 211-1K vs. 321-2K; the latter is observed in AFM, and also in DMA.

These observations are consistent with the deformation-induced glass transition mechanism proposed by Bogoslovov
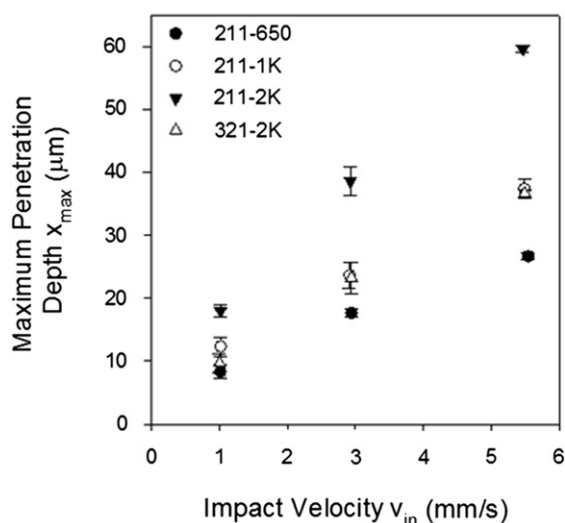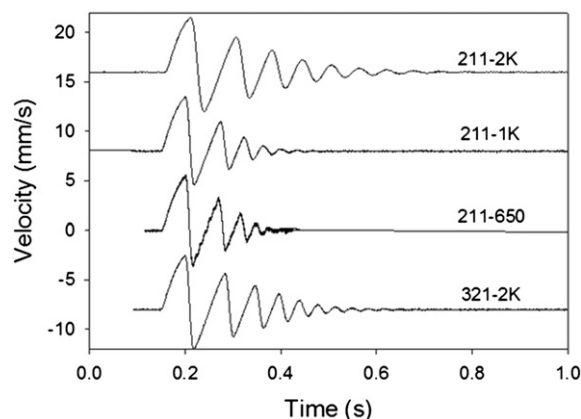

Fig. 9. Comparison of impact indentation damping characteristics obtained at a velocity of 5.5 mm/s for 211-650, 211-1K, 211-2K, and 321-2K [data offset vertically for ease of differentiation among samples].
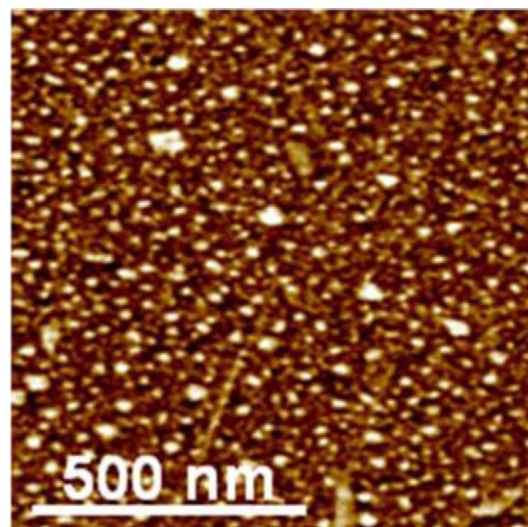

Fig. 10. AFM-phase image of 321-2K (50° light-to-dark).

et al., wherein the calorimetric T_g close to operation temperature is a prerequisite for enhanced energy-dissipation in polyurea [2]. Furthermore, it is envisioned that the formation of a three-dimensional interconnected fibrillar-like microstructure which consists of intermolecular hydrogen-bonds is also the key to facilitating impact damping.

4. Conclusion

We have investigated and elucidated the molecular influence on tunable microstructure of select model PUUs. AFM-phase imaging and AFM-modulus mapping have shown capability to identify the morphology as a function of soft segment M_w: 2K, 1K, and 650 g/mol. Results show that changing SS M_w from 2000 g/mol to 650 g/mol while keeping the same molar ratio of HMDI:PMTO:DETA results in PUUs ranging from microphase-separated to phase-mixed microstructure. AFM imaging enabled visualization of the microstructural details, not available through scattering techniques. It was found that the degree of microphase separation can vary between the as-cast surface and in the bulk. However, it is shown that the degree of microphase separation in the 211-2K is comparatively high in both the bulk and surface when compared with the 211-1K and 211-650. AFM-modulus mapping also

Fig. 8. Plots of maximum indentation depth as a function of impact velocity obtained for 211-650 (●), 211-1K (○), 211-2K (▼) and 321-2K (△).

highlighted very detailed distinct microstructures which are not as prevalent in the AFM-phase image. In 211-2K, it was noted the presence of phase-mixed regions, in addition to the SS-rich domain, which corroborates well with the DMA tan δ data. Interestingly, the 211-1K exhibited surface microstructure that differed from its bulk counterpart and included fibrillar-like microstructure.

The overall AFM-modulus also increased, as soft segment length decreased, consistent with nanoDMA data as well as with storage modulus data from dynamic mechanical analysis. AFM-modulus tended to be slightly higher than both the nanoDMA storage modulus and DMA storage modulus, which is presumably due to the rate-dependent characteristic of PUUs in response to 1 Hz in DMA and $\sim$100 Hz in nanoDMA vs. $\sim$10^5 Hz in AFM. Sample 211-650 exhibited not only the highest modulus data but also the fastest damping of the impact response among all PUUs considered. The enhanced damping capability is partly a result of a shift of SS T_g (from DMA) much closer to room temperature.

The molecular influence on impact damping response was further validated by comparing PUUs of similar hard segment contents but varying the SS M_w; greater phase mixing gives rise to shorter damping times in 211-1K over 321-2K. Based on these observations we have demonstrated pathways via exploiting enabling molecular mechanisms for best use of the versatile chemistry of PUU in the design of next-generation hierarchical elastomeric materials to achieve optimized physical and mechanical properties for soldier protection.

Acknowledgments

References

[1] Holden G, Legge N, Quirk R, Schroeder H. Thermoplastic elastomers. 2nd ed. Munich: Hanser Publishers; 1996.
[2] Bogoslovov RB, Roland CM, Gamache R. Appl Phys Lett 2007;90:221910–221910-3.
[3] Tekalur SA, Shukla A, Shivakumar K. Composite Structures 2008;84:271.
[4] Bahei-El-Din YA, Dvorak GJ, Fredricksen OJ. Int J Solid Structures 2006;43:7644.
[5] Porter JR, Dinan RJ, Hammons MI, Knox KJ. AMPTIAC Quart 2002;6:47.
[6] Roland C, Fragiadakis D, Gamache R. Composite Structures 2009;92:1059–64.
[7] Fragiadakis D, Gamache R, Bogoslovov RB, Roland CM. Polymer 2010;51:178–84.
[8] Grujicic M, Pandurangan B, He T, Cheeseman BA, Yen C-F, Randow CL. Mater Sci Eng A 2010;527:7741–51.
[9] Yi J, Boyce MC, Lee GF, Balizer E. Polymer 2006;47:319–29.
[10] Sarva S, Deschanel S, Boyce MC, Chen W. Polymer 2007;48:2208–13.
[11] Samuels SL, Wilkes GL. J Polym Sci Symposia 1973;43(1):149–78.
[12] Wang CB, Cooper SL. Macromolecules 1983;16:775–86.
[13] Kojio K, Furukawa M, Motokucho S, Shimada M, Sakai M. Macromolecules 2009:8322–7.
[14] Sheth JP, Aneja A, Wilkes GL, Yilgor E, Atilla GE, Yilgor I, et al. Polymer 2004:6919–32.
[15] Hernandez R, Weksler J, Padsalgikar A, Choi T, Elena Angelo E, Lin JS, et al. Macromolecules 2008;41:9767–76.
[16] Yilgor I, Yilgor E. Polym Rev 2007;47:487–510.
[17] Aneja A, Wilkes GL. Polymer 2003;44:7221–8.
[18] Aneja A, Wilkes GL. Polymer 2004;45:927–35.
[19] Yilgor E, Isik M, Yilgor I. Macromolecules 2010;43:8588–93.
[20] Korley LTJ, Pate BD, Thomas EL, Hammond PT. Polymer 2006;47:3073–82.
[21] Sheth JP, Wilkes GL, Fornof AR, Long TE, Yilgor I. Macromolecules 2005;38:5681–5.
[22] O'Sickey MJ, Lawrey BD, Wilkes GL. J Appl Poly Sci 2003;89:3520–9.
[23] O'Sickey MJ, Lawrey BD, Wilkes GL. J Appl Poly Sci 2002;84:229–43.
[24] Garrett JT, Runt J, Lin JS. Macromolecules 2000;33:6353–9.
[25] Garrett JT, Siedlecki CA, Runt J. Macromolecules 2001;34:7066–70.
[26] Sheth JP, Unal S, Yilgor E, Yilgor I, Beyer FL, Long TE, et al. Polymer 2005;46:10180–90.
[27] Koevoets RA, Versteegen RM, Kooijman H, Spek AL, Meijer EW. J Am Chem Soc 2005;127:2999–3003.
[28] Pathak JA, Twigg JN, Nugent KE, Ho DL, Lin EK, Mott PH, et al. Macromolecules 2008;41:7543–8.
[29] Sarva S, Hsieh AJ. Polymer 2009;50:3007–15.
[30] Rinaldi R, Hsieh AJ, Boyce MC. J Polym Sci Polym Phys 2011;49:123–35.
[31] Hsieh AJ, Yu JH, Rinaldi R, Krogman KC, Hammond PT, Boyce MC. In: Proc. 27th army science conference 2010, Orlando, FL.
[32] Christenson EM, Anderson JM, Hiltner A, Baer E. Polymer 2005;46:11744–54.
[33] Rinaldi RG, Boyce MC, Weigand SJ, Londono DJ, Guise MW. J Polym Sci Part B Polym Phys 2011;49:1660–71.
[34] Yeh F, Hsiao BS, Sauer BB, Michel S, Siesler HW. Macromolecules 2003;36:1940–54.
[35] Schön P, Dutta S, Shirazi M, Noordermeer J, Vancso JG. J Mater Sci 2011;46:3507–16.
[36] Schön P, Bagdi K, Molnár K, Markus P, Pukánszky B, Vancso JG. Eur Polym J 2011;47:692–8.
[37] Sahin O. Rev Sci Instrum 2007;78:103707–11.
[38] Constantinides G, Tweedie C, Holbrook D, Barragan P, Smith JF, Van Vliet KJ. Mater Sci Eng A 2008;489:403–12.
[39] Constantinides G, Tweedie CA, Savva N, Smith JF, Van Vliet KJ. Exp Mechanics 2009;49:511–22.
[40] Kalcioglu ZI, Qu M, Strawhecker KE, Shazly T, Edelman E, VanLandingham MR, et al. Philosophical Magazine 2011;91:1339–55.
[41] Hsieh AJ, Strawhecker KE. PMSE preprints of the American Chemical Society, vol. 105. Denver, CO: American Chemical Society; 2011. p. 162–3.
[42] Chantawansri TL, Hsieh AJ. ARL Director's research initiative program progress report, ARL-MR-0800; 2012.